Outline for
a Deeply Virtual Compton Scattering Experiment
using COMPASS at CERN

E. Burtin, N. d'Hose, P.A.M. Guichon, S. Kerhoas-Cavata, J. Marroncle, L. Mossé, ...

DAPNIA-SPhN, CEA-Saclay, F91191 Gif-sur-Yvette Cedex

...

...

Abstract

We propose to use the 190 GeV (or 100 GeV) muon beam at CERN to study Deeply Virtual Compton Scattering in the Bjorken regime ($Q^2 \geq 1.5$ GeV^2 and $0.03 \leq x_{Bj} \leq 0.27$) after the COMPASS program is achieved. The Q^2, x_{Bj}, ϕ and t dependence analysis of this reaction holds out the promise to access the Generalized Parton Distributions of the nucleon. The goal of this letter is to provide a first estimate of the counting rates in a sensible and large acceptance in Q^2 and x_{Bj} available with this apparatus. We also discuss the experimental implications for the present COMPASS set-up as well as the required complementary equipments. The estimation of the cross section of the competing channels (deep meson production) is in progress and should be finished at the time of presenting a full fledged proposal. A study of the final outcome of this experiment is also underway.

1 Introduction

Much of the internal structure of the nucleon has been revealed during the last three decades through the inclusive scattering of high energy leptons on nucleons in the Bjorken or Deep Inelastic Scattering (DIS) regime. Simple theoretical interpretations of the experimental results and quantitative conclusions can be reached in the framework of the parton model and QCD because one sums over all possible final hadronic states. For instance, unpolarized DIS led to the discovery of the quark and gluon substructure of the nucleon, with the quark carrying about half of the nucleon's momentum. Furthermore, polarized DIS revealed that only about 25% of the spin of the nucleon is carried by the quark's intrinsic spin. Presently a large effort is devoted to the measurement of the contribution of gluon's intrinsic spin using COMPASS, RHIC and HERMES. A remaining part to solve the nucleon spin puzzle is to determine the quark (and gluon) orbital angular momentum contribution to the nucleon spin.

The recent developed formalism of "Generalized Parton Distributions" (GPDs) [1, 2] emphasized that such a piece of information can be obtained in hard exclusive leptoproduction experiments. The GPDs contain information on the interference between different quark configurations, on the quark's transverse momentum distribution, as well as on their angular momentum distribution. GPDs provide a unifying picture for an entire set of fundamental quantities of hadronic structure, such as: the vector and axial nucleon form factors, the polarized and unpolarized parton distribution, and the spin components of the nucleon due to orbital excitations. More than 150 theoretical papers have been published on these topics since 1996.

Deeply Virtual Compton Scattering (DVCS) is one of the favorite reactions to measure the GPDs because it is the simplest process that can be described in terms of GPDs. We propose to measure DVCS at COMPASS and to take advantage of the very high energy of the muon beam to investigate a large kinematical domain in x_{Bj} and Q^2. The DVCS cross section will be mapped from $Q^2 = 1.5$ to 6.5 GeV^2 and $x_{Bj} = 0.03$ to 0.27. The 190 GeV muon energy assure the DVCS to be dominant compared with the Bethe-Heitler process. Nevertheless for the smallest values of x_{Bj} we can also use a smaller energy of 100 GeV to study the interference term between BH and DVCS, which will give information on Compton scattering at the amplitude level, rather than probabilities.

Complementary studies can also be done such as the longitudinal leptoproduction of vector and pseudoscalar mesons in order to take benefit of the whole COMPASS set-up and to enlarge the scope of the experiment with respect to the physics of the GPDs.

2 Motivations for a DVCS experiment

2.1 Phenomenology of the GPDs

In this section we briefly review the formalism and the properties of the Generalized Parton Distributions (GPDs). We recall that in DIS regime (defined by an incoming virtual photon γ^* of characteristics $Q^2, \nu \rightarrow \infty$ and $x_{Bj} = Q^2/2m_N\nu$ finite), the ordinary parton distribution $q(x)$ gives the probability for finding a parton q carrying a longitudinal momentum fraction x in the fast moving proton. The standard approach is to write the DIS cross section using the optical theorem as the imaginary part of the forward virtual Compton amplitude. The imaginary part selects just the $x = x_{Bj}$ value from the x loop integral.

$$\sigma_{DIS} = \sum_X |\gamma^* p \rightarrow X|^2 \quad \propto \quad \mathcal{I}m(\gamma^* p \rightarrow \gamma^* p)_{t=0} = \sum_q e_q^2 [xq(x)]_{x=x_{Bj}} \tag{1}$$

Deeply Virtual Compton Scattering is a natural extension of the previous case with the difference that the final proton receives a momentum transfer Δ, which gives skewedness compared with the inclusive case. Ji [1], Radyuskin [2] and Collins [3]

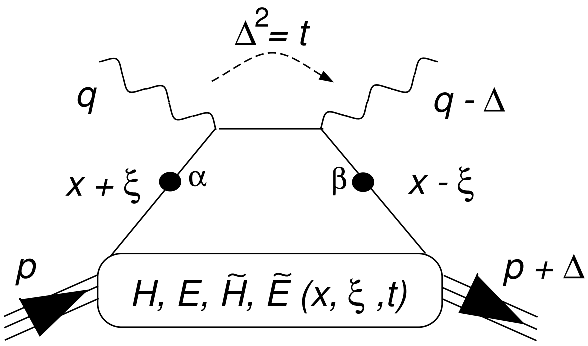

Figure 1: *Handbag diagram for DVCS.*

have shown that the deeply virtual Compton scattering in the forward limit can be factorized in leading-order pQCD into a hard-scattering part (exactly calculable in pQCD) and a non-perturbative nucleon structure part, as illustrated in Fig. 1. In the so-called "handbag" diagram, the lower glob represents the soft structure of the nucleon and can be described, at leading order in $1/Q$, in terms of four Generalized Parton Distributions, which conserve quark helicity. They are $H, \tilde{H}, E$ and $\tilde{E}$ and depend upon three kinematical variables: x, ξ and t. x is the average longitudinal momentum fraction of the active quarks in the quark loop. ξ is the longitudinal momentum fraction of the transfer Δ, and is related to x_{Bj} ($\xi = x_{Bj}/(2-x_{Bj})$ in the Bjorken limit). $t = \Delta^2$ is the transfer between the virtual and real photons.

The condition for factorization is t small ($t \leq 1$ GeV^2). Indeed the transverse transfer $\Delta_\perp$ has to be small enough so that the outgoing real photon escapes with the maximum energy and momentum without disturbing the spectators and so, the unscattered spectator partons have a good overlap with the outgoing proton and flow right through.

Precisely, the light-cone matrix element of the bilocal operator that enters in the hard leptoproduction reactions (represented by the lower blobs in Fig. 1) is at leading twist in Q^2 given by:

$$\begin{aligned}
&\frac{P^+}{2\pi}\int dy^- e^{ixP^+y^-} < p'|\bar{\Psi}_\beta(-\tfrac{y}{2})\Psi_\alpha(\tfrac{y}{2})|p> |_{y^+=\vec{y}_\perp=0} \\
&\quad = \frac{1}{4}\Big\{(\gamma^-)_{\alpha,\beta}\Big[H^q(x,\xi,t)\bar{N}(p')\gamma^+N(p) + E^q(x,\xi,t)\bar{N}(p')i\sigma^{+\kappa}\tfrac{\Delta_\kappa}{2m_N}N(p)\Big] \\
&\quad + (\gamma_5\gamma^-)_{\alpha,\beta}\Big[\tilde{H}^q(x,\xi,t)\bar{N}(p')\gamma^+\gamma_5 N(p) + \tilde{E}^q(x,\xi,t)\bar{N}(p')\gamma_5\tfrac{\Delta^+}{2m_N}N(p)\Big]\Big\} \qquad (2)
\end{aligned}$$

where $\Psi_{\alpha,\beta}$ are the quark field, N the nucleon spinor, q is a quark flavor index and $P = (p + p')/2$.

This formula explicitly shows the vector (axial) nature of $H, E, (\tilde{H}, \tilde{E})$ GPDs associated or not with the γ_5 matrix. The H and $\tilde{H}$ are generalizations of the parton distributions measured in deep inelastic scattering. In the forward limit (corresponding to $\xi = 0$ and $t = 0$) H^q reduces to the quark distribution $q(x)$ and $\tilde{H}^q$ to the quark-helicity distribution $\Delta q(x)$ measured in DIS. H_q and $\tilde{H}_q$ conserve the helicity of the proton, whereas E_q and $\tilde{E}_q$ allow for the possibility that the proton helicity is flipped [4]. In such a case the overall helicity is not conserved: the proton changes helicity but the massless quark does not, so that angular momentum conservation implies a transfer of orbital angular momentum. This is only possible for nonzero transverse momentum transfer, and therefore cannot be observed with ordinary parton distributions. That the GPDs involve the orbital angular momentum of the partons is epitomized in the Ji's sum rule [1], which states that the second moment

$$\frac{1}{2}\sum_q \int_{-1}^{+1} dx x(H^q(x,\xi,t=0) + E^q(x,\xi,t=0)) = J^{quark} \qquad (3)$$

at $t = 0$ gives the total (spin + orbital) angular momentum carried by the quarks.

In the parton interpretation, the quark going out of the parent hadron carries the longitudinal momentum fraction $x + \xi$, while the longitudinal momentum fraction of the returning quark is $x - \xi$. The GPDs represent the interference between the wave functions representing these two different nucleon states. GPDs thus correlate different parton configurations in the hadron at the quantum mechanical level. The kinematical regime $|x| \leq \xi$ where the initial hadron emits a quark-antiquark or gluon pair (or a meson) has no counterpart in the usual parton distributions and carries information about the $q - \bar{q}$ and gg components in the hadron wave function.

The first moments of the GPDs are related to the standard hadronic form factors.

$$\begin{aligned}
&\sum_q e_q \int_{-1}^{+1} dx H^q(x,\xi,t) = F_1(t), \qquad &&\sum_q e_q \int_{-1}^{+1} dx \tilde{H}^q(x,\xi,t) = g_A(t), \\
&\sum_q e_q \int_{-1}^{+1} dx E^q(x,\xi,t) = F_2(t), \qquad &&\sum_q e_q \int_{-1}^{+1} dx \tilde{E}^q(x,\xi,t) = h_A(t). \qquad (4)
\end{aligned}$$

where e_q is the electric charge of the relevant quark. F_1, F_2 are the Dirac and Pauli form factors respectively, g_A is the axial form factor and h_A is the induced pseudoscalar form factor. A simple physical interpretation of GPDs thus emerges [5, 6]: they quantify the contribution of quarks with longitudinal momentum fraction x to the corresponding form factor. Given the fact that one can associate the Fourier transform of form factors with charge distributions in position space, it is very tempting to expect that GPDs also contain some information about the distribution of partons in position space. It is clearly established [5] that for purely transverse transfer $\xi = 0$, $H(x, 0, -\Delta_\perp^2)$ is the Fourier transform of the probability density to find a quark with momentum fraction x at a given distance $b_\perp$ from the center of momentum in the transverse plane: $H(x, 0, -\Delta_\perp^2) = \int d^2 b_\perp e^{-i\Delta_\perp \cdot b_\perp} f(x, b_\perp)$. Consequently the width of the $b_\perp$ distribution goes to zero as $x \to 1$ since the active quark becomes the center of momentum. In momentum space this implies that $H(x, 0, t)$ should become t-independent as $x \to 1$. At a more qualitative level, one expects quarks at large x to come from the more localized valence "core" of the hadron, while the small x region should receive contributions from the much wider meson "cloud" and therefore one would expect a gradual increase of the t-dependence of $H(x, 0, t)$ as one goes from larger to smaller values of x.

There are two approaches used to model GPDs. One is based on a direct calculation using the definition (2) in specific dynamical models, such as bag model [7], chiral soliton model [8], light-cone formalism [9], etc. Another approach is a phenomenological construction [10] based on reduction formulas relating GPDs to usual parton densities $q(x)$, $\Delta q(x)$ and form factors $F_1(t), F_2(t), G_A(t), h_a(t)$. The most complete construction is presented in the references [11, 12].

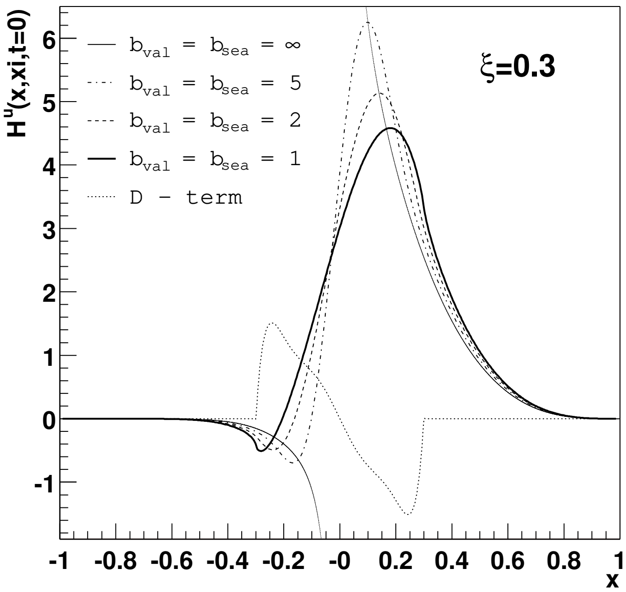

Figure 2: *Prediction of the GPD* $H^u(x, \xi, t = 0)$ *and* $\xi = 0.3$ *and sensibility to different components (see the comments in the text) (Figure from Ref.[12])*

The x and ξ dependencies are presented in Fig. 2 in a phenomenological approach [12]. The parametrization of $H^u(x, \xi, t = 0)$ has two components. The first component is based on the double distribution representation of Radyuskin [11]) and depends on a parameter b which characterizes the strength of the ξ dependence of the GPD. The limiting case $b \to \infty$ corresponds to the ξ independent ansatz for the GPD, i.e. $H^u(x, \xi, t = 0) = u(x)$, the ordinary u-quark distribution (thin full curve). The exponent b is a free parameter for the valence contribution (b_{val}) and for the sea contribution (b_{sea}) to the GPD, which can be used as fit parameters in the extraction of the GPDs from the experimental observables. The second component is the so-called D-term which allows the GPDs to fulfill the polynomial conditions [13]. In Fig. 2 we show the D-term (dotted curve) calculated in the quark soliton model [8] in the regime $|x| \leq \xi$, which strongly resembles meson distribution amplitudes. This term is linked to the spontaneously broken chiral symmetry of QCD and mainly determined by the contribution of the pion cloud. The two components (double distribution and D-term) should be added to get the full GPD $H^u(x, \xi, t = 0)$.

The simplest parametrization of the t dependence of the GPD consists of the factorized ansatz: $H^u(x, \xi, t) = H^u(x, \xi, t = 0)F_1^u(t)/2$ where $F_1^u(t)$ represents the elastic Dirac form factor for the quark flavor u in the nucleon. Nevertheless as stated above in the geometric description, $H(x, \xi = 0, t)$ should become t-independent as $x \to 1$. A reasonable description of the parton structure suggests a transverse size of hadrons that grows like: $< b_\perp^2 >= \alpha ln \frac{1}{x}$ (α is a free parameter). This implies an unfactorized ansatz: $H(x, \xi = 0, t) = q(x)e^{t<b_\perp^2>} = q(x)\frac{1}{x^{\alpha t}}$. We see the influence of these two ansatz in Fig. 5 notably for a small x_{Bj} value where the effect is enhanced.

2.2 Deeply virtual Compton scattering

Deeply virtual Compton scattering (DVCS) is the key reaction to determine the GPDs experimentally. This process is accessed by lepton scattering $lp \to l'p'\gamma'$. In this reaction, the final photon can be emitted either by the leptons or by the proton (see Fig. 3). The last process is the process of interest, while the first one is described by the Bethe-Heitler (noted BH) amplitude which is completely calculable in QED. The BH

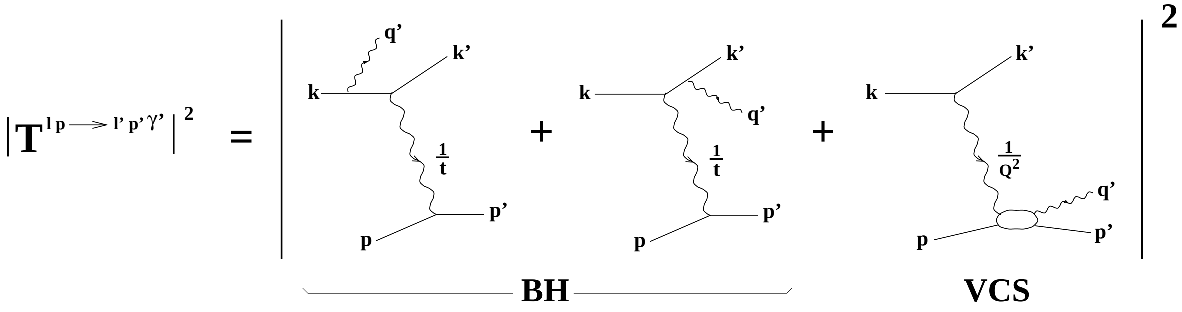

Figure 3: *BH and VCS amplitudes*

propagator goes like $1/t$ while the DVCS one goes like $1/Q^2$. Therefore the interesting region indicated in Fig. 4, large Q^2, small t ($t \leq 1$ GeV^2) favors the BH process. To overcome this problem the only way is to go up in energy to increase the virtual photon flux of the DVCS process.

Figure 4 illustrates this fact. With the very high energy 190 GeV muon beam available at CERN, the DVCS contribution dominates clearly the BH process at large Q^2 and in a large range of x_{Bj}. This dominance effect decreases when Q^2 increases, or x_{Bj} decreases. So at COMPASS kinematics, $x_{Bj} \simeq 0.05$ seems to be the lower limit.

However the interference between BH and DVCS offers a unique possibility to study Compton scattering at the amplitude level. If we use a longitudinally polarized lepton

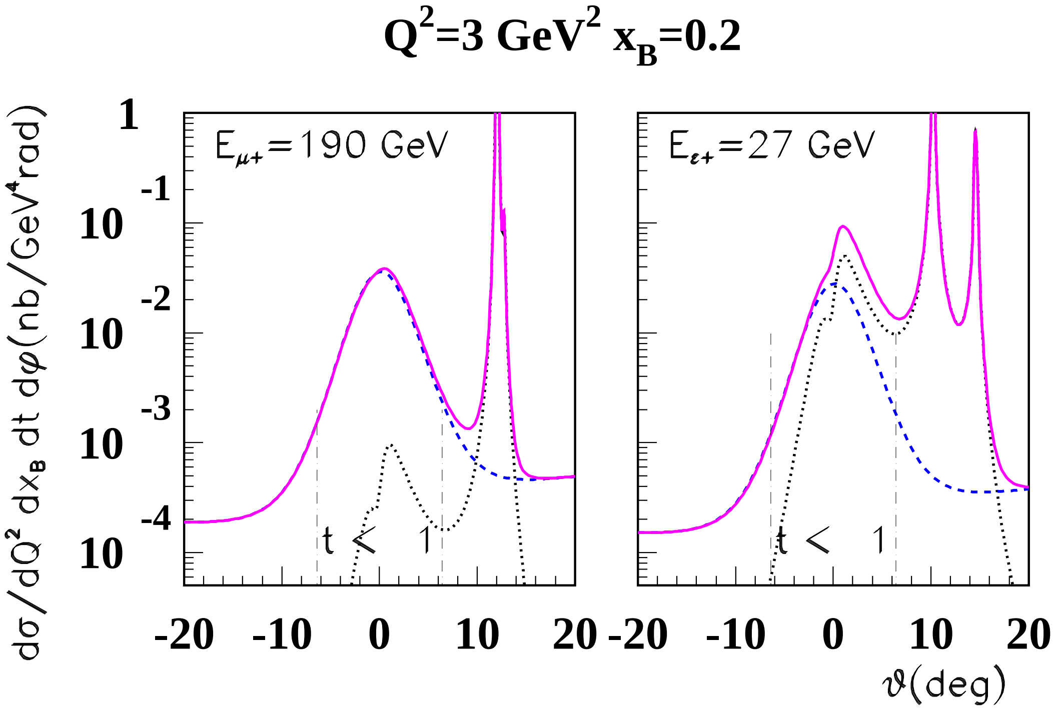

Figure 4: *Cross sections for the photon leptoproduction $lp \to l'p'\gamma$ as a function of the photon angle. Comparison between BH (dotted lines), DVCS (dashed lines) and total cross sections (full lines) for 2 energies of the leptons, 27 GeV for the HERMES positron beam energy and 190 GeV for the COMPASS muon beam energy.*

beam, the helicity-dependent interference term is proportional to the imaginary part of the DVCS amplitude and this selects the GPDs at the specific value $x = \xi$. If we use a lepton beam with two possible charge states, the charge-dependent interference $\sigma_{l+} - \sigma_{l-}$ term is then proportional to the real part of the DVCS amplitude which is sensitive to the complete dependence on x of the GPDs, notably away from the line $x = \xi$ [1]. We can note that it is very suitable to use the positive and negative muon beams available at CERN at a lower energy of 100 GeV to increase the interference effect.

The large sensibility of the beam charge asymmetry [14] to the different components of the GPDs is clearly shown in Fig. 5. The pronounced ϕ dependence of the charge asymmetry provides a useful observable to study the D-term contribution to the GPDs and their t dependence.

2.3 Deep meson production

The GPDs reflect the structure of the nucleon independently of hard probe. In this sense, they are universal quantities and can also be accessed, in different flavor combinations, through the hard exclusive production of meson $(\pi^0, \rho^0, \omega, \phi, ...)$ for which a factorization proof has been given in [3]. The factorization applies when the virtual photon is longitudinally polarized because in this case, the end-point contributions in

[1] The same remark is true for the total cross section, but we have no information on the phase.

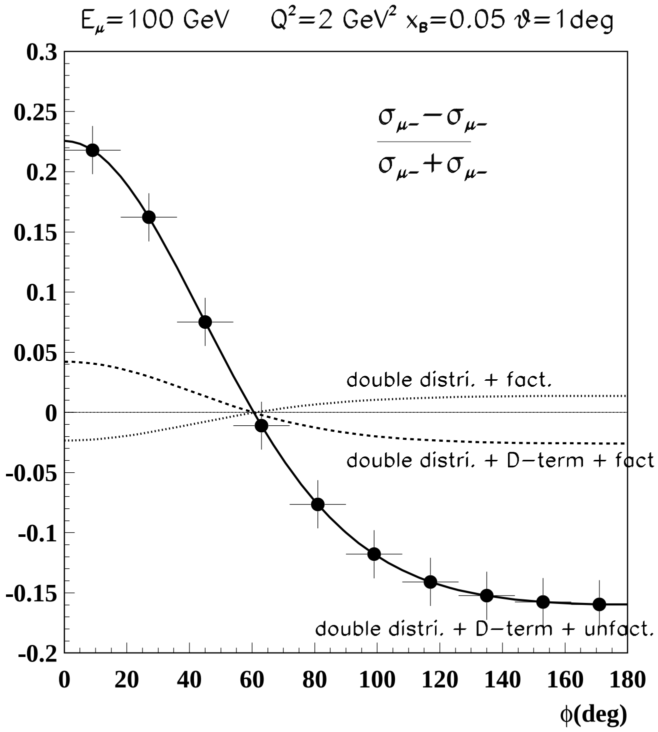

Figure 5: *Beam charge asymmetry for* $E_\mu = 100GeV$*,* $x_{Bj} = 0.05$*,* Q^2*=2* GeV^2*, and* $t = -0.15GeV^2$*. The effect of the different components of the GPDs is clearly indicated. Dotted line: GPDs calculated according to the double* (x, ξ) *distribution (with* $b_{val} = b_{sea} = 1$*) and the factorized ansatz for the* t *dependence. Dashed line: GPDs calculated according the same assumptions, but including the D-term. Full line: GPDs calculated according to the double* (x, ξ) *distribution plus the D-term, and the unfactorized ansatz for the* t *dependence (with* $\alpha = 0.8$*). The experimental points with the error bars are indicated for an experiment at COMPASS described in the* 3^{rd} *paragraph. The size of the bins is determined for* $Q^2 = 2 \pm 0.5$ GeV^2*,* $x_B = 0.05 \pm 0.02$ *and* $0.06 \leq |t| \leq 0.3$ GeV^2*. 3 months of data taking are considered for each* μ^+ *and* μ^- *beam with a muon flux of* 2.10^8 *per spill.* μ^+ *and* μ^- *are naturally polarized. At COMPASS for a given hadron setting they have an opposite polarization, i.e.* $P_{\mu^+} = -0.8$*,* $P_{\mu^-} = +0.8$ *and the effect of the polarization in the beam charge assymetry vanishes.*

the meson wave function are power suppressed. It has also been shown in [3] that the leading order pQCD predicts that the vector meson channels $(\rho^0_L, \omega_L, \phi_L)$ are sensitive only to the vector GPDs (H and E) whereas the pseudoscalar channels $(\pi^0, \eta, ...)$ are sensitive only to the axial GPDs ($\tilde{H}$ and $\tilde{E}$). It is clear that it is important to investigate at the same time these complementary channels. Some work on these studies at COMPASS has already been undertaken [15, 16].

2.4 Experimental plans in the world

With the very high centre of mass energy available at the HERA collider (27 GeV positron beam and 820 GeV proton beam), first observation of DVCS have been reported at ZEUS [17] and H1 [18]. The very small values of x_{Bj} $(0.0005 \leq x_{Bj} \leq 0.01)$

of these events suggest that they probe mainly the gluon content of the proton. Moreover the lack of exclusivity certainly affects the interpretation of these events in terms of exclusive DVCS, that is in terms of GPDs.

At HERMES, with the 27 GeV positron beam, production of longitudinal ρ^0_L has shown a significant contribution of the quark GPDs in a domain of x_{Bj} close to 0.1 [19]. Preliminary beam polarization asymmetries have also been obtained [20]. Nevertheless the final state baryon is not unambiguously constrained to be a proton (Δ or other resonance may also contribute to the signal). To remedy this situation the implementation of a recoil detector is already foreseen in the next coming years.

Two experiments [21, 22] have been approved for the very next years at 6 GeV at Jefferson Laboratory to study the exclusive electroproduction of photons and mesons and another one [23] will be presented very soon. They will investigate mainly the regime of $x_{Bj} \simeq 0.35$. Longitudinal meson production will be studied with the large acceptance CLAS detector while DVCS will be investigated through interference with the Bethe-Heitler in both experimental halls (with CLAS or with a high resolution spectrometer plus a calorimeter). A recent evidence of a DVCS/BH interference has been provided with CLAS and the corresponding beam polarization asymmetry is under publication [24].

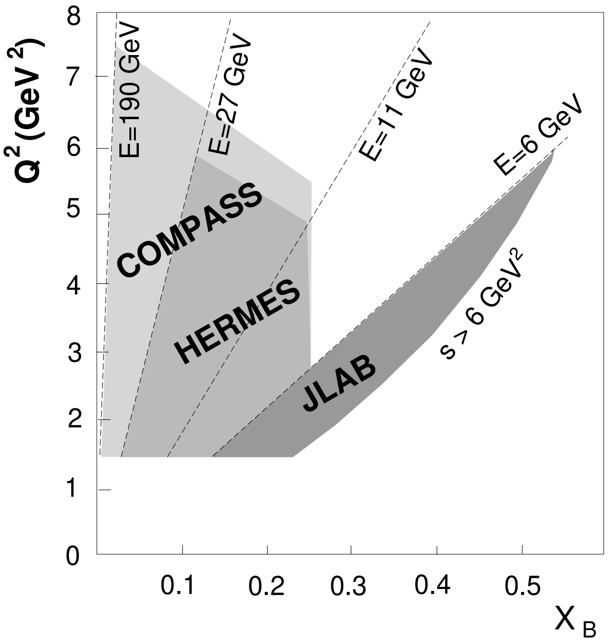

Figure 6: *Kinematical coverage for various planned or proposed experiments. The limit* $s \geq 6$ *GeV*^{2} *assures to be above the resonance domain, and* $Q^2 > 1.5$ *GeV*^{2} *allows to reach the Deep Inelastic regime.*

Figure 6 shows the accessible domain in Q^2 and x_{Bj} for a given maximum lepton energy. The low energy of Jlab offers only a restricted domain. Nevertheless the energy will be extended to 11 GeV, and the very comfortable luminosity ($\mathcal{L} \geq 10^{34}$ cm^{-2}s^{-1}) will allow a good investigation of the regime $0.2 \leq x_{Bj} \leq 0.4$. COMPASS provides the only way to go to small x_{Bj} with a large range Q^2 Typically:

$$0.03 \leq x_{Bj} \leq 0.27$$

$$1.5 \leq Q^2 \leq 6.5\mathrm{GeV}^2$$

2.5 Goal of a DVCS experiment at COMPASS

The very high energy of the muon beam available at COMPASS allows to perform experiments

- either with a μ^+ beam at $E_\mu = 190$ GeV to measure the total DVCS cross section (which dominates clearly the Bethe-Heitler process)
- or with both μ^+ beam and μ^- beam at $E_\mu = 100$ GeV in order to measure a beam charge assymetry and thus to play with the BH-DVCS interference which offers the unique possibility to reach the DVCS amplitude.

A complete DVCS experiment will measure the evolution of the cross section as a function of the kinematical variables Q^2, x_{Bj}, t and ϕ the angle between the lepton and hadron planes. The study of the ϕ angular distribution evolution with Q^2 will test the handbag dominance, the importance of the D-term (linked to chiral properties on GPDs) and will rate relative contributions of the higher twists [25]. A precise study of the t evolution at different x_{Bj} would give access to the parton distributions as a function of the position in the transverse plane. This is a new feature with respect to DIS where only the average in the transverse plane is measured. One expects quarks at large x_{Bj} to come from the more localized valence "core" of the hadron, while the small x_{Bj} should also receive contributions from the much wider meson "cloud" and therefore one would expect a gradual increase of the t dependence as one goes from larger to smaller values of x_{Bj} [5, 6].

It is clear that a complete experiment including DVCS and meson production at COMPASS allows the investigation of the GPDs in the largest kinematical domain in Q^2 and x_{Bj} and at the smallest value of x_B ever reached by the other facilities with fixed target. However these experiments will come in some year from now and so, it is really important to determine the impact of such experiments within their accuracies (due to the modest luminosity of COMPASS). It is necessary to quantify the constraints on the GPDs, for example on E^q (which is maybe the most unknown GPD) provided by such an experiment. Among others, a really ambitious goal is to demonstrate how much the knowledge of the angular momentum carried by quarks, is improved by a COMPASS experiment. This work remains to be done.

3 Realization of a DVCS experiment at COMPASS

In this section we focus on the best suitable realization of a DVCS experiment in the COMPASS environment. We plan to detect the exclusive reaction:

$$\mu p \to \mu' p' \gamma$$

in the kinematical regime of interest defined in the previous section:

$$0.03 \leq x_{Bj} \leq 0.27$$
$$1.5 \leq Q^2 \leq 6.5\mathrm{GeV}^2$$
$$0.058 \leq |t| \leq .5\mathrm{GeV}^2 \text{ that means }^{2}\ 250 \text{ MeV/c} \leq P_p \leq 750 \text{ MeV/c}$$
$$\text{a complete coverage in } \phi.$$

The first subsection reports on the request of the highest luminosity reachable at COMPASS and the resulting counting rates that we can expect for such an experiment. This concerns directly the stakes which were presented in the last section: the possibility to clearly disentangle models of GPDs and to provide a significant impact on important questions as the determination of the angular momentum carried by the quarks.

The following subsections present the experimental procedure to select the exclusive DVCS channel and the different pieces of detection that are required. They are mostly part of the COMPASS set-up: muon detection which insures a good resolution in x_{Bj} and Q^2, photon detection with a reorganization of the electromagnetic calorimeter ECAL1 and ECAL2. However it is necessary to add an extra recoil detector to collect the recoil proton and to insure the exclusivity by a good rejection of additional particles. First tests of the detection of recoil protons are also reported.

3.1 Luminosity and counting rates

3.1.1 Muon beam and intensity

The experiment will use 100-190 GeV/c muons from the M2 beam line. Limits on SPS operation, production target safety and radioprotection in the experimental hall imply that the maximum flux of muon to be expected is of $2\,10^8$ muons per SPS spill. Moreover, the SPS will have to be shared with filling of the LHC and extraction for CNGS resulting in a 27 seconds SPS "super cycle"[26] and a 3.5 seconds spill duration for the North Area experiments. Under these circumstances, we will have two possibilities for data taking conditions :

	SPS cycle	average flux	instantaneous flux
CNGS running	3.5 s / 27 s	$0.7\,10^7 \mu/s$	$5.7\,10^7 \mu/s$
CNGS not running	5.2 s / 16.8 s	$1.2\,10^7 \mu/s$	$3.8\,10^7 \mu/s$

[2] we plan to have a minimum proton detection at 250 MeV/c which does not allow to reach exactly the minimal value of t

We plan on running with both μ^+ and μ^- at the highest intensity which would certainly be achieved for a beam of 100 GeV/c[27]. Muons are provided by pion and kaon decay and are naturally polarized. If we keep the ratio of muon and hadron momenta and the collimator settings the same (both the collimator settings in the hadron section of the beam and the scrapper settings in the muon part) the μ^+ and μ^- polarizations should be equal to a very good precision, i.e. $P_{\mu+} = -0.8$ and $P_{\mu-} = +0.8$. However the flux will be different, i.e. $N_{\mu+} = 2.10^8$ per spill and $N_{\mu-} = 10^8$ per spill. We can maximize the two muon flux by playing differently with the collimators and the lenghts of the Be target which gives rise to the pions and kaons from the SPS proton beam. Then the slight difference in the two polarizations should be taken into account but will affect hardly the beam charge assymetry[14].

The beam spot size (RMS) at the centre of the target is 4.5 mm in the horizontal direction and 7.5 mm in the vertical direction[27].

3.1.2 Liquid hydrogen target

We plan to use a 2.5 meter long liquid hydrogen target of cylindrical shape. The corresponding density is 18 g/cm^2 and gives a luminosity of 1.3 10^{32} cm$^{-2}s^{-1}$ (for a duration spill of 16.8s). It is important to study the influence of a longer target in order to increase significantly the luminosity. We recall that the EMC liquid hydrogen target was 6 meter long.

The radius of the planned target is 3 cm, corresponding to 4 times the biggest transverse dimension of the beam spot. We consider safe target walls and insulation equivalent to 3 mm of scintillator. With this design the lowest momentum for protons to escape the target and to reach the time of flight detection system (i.e. to go through 4 additional mm of scintillator) is 264 MeV/c at 90 deg. and 284 MeV/c at 50 deg. (which is about the minimum angle of a DVCS recoil proton). R&D has to be done to find the compromise between the minimization of the target wall thickness, the maximization of the target length and the safety requirement.

3.1.3 Counting rates

A simulation has been performed to estimate the DVCS counting rates. A complete set of detector, which will be described below, are considered in order to match as well as possible the phase space which originates from the chosen kinematical domain in Q^2, X_{Bj} and t. The simulation includes a kinematical phase space generator and the calculation of theoretical cross sections, performed by L. Mossé, P.A.M. Guichon and M. Vanderhaeghen [14]. It takes into account both DVCS and BH processes.

The following tables present the number of events collected with a 100% overall efficiency for:

$\mathcal{L} = 1.5\ 10^{32}$ cm^{-2}s^{-1} (1.4. 10^7 muons/s and a 2.5m long hydrogen target)
$0.058 \leq |t| \leq .5\text{GeV}^2$ that means 250 MeV/c $\leq P_p \leq$ 750 MeV/c
a complete coverage in ϕ

1. for μ^+ at $E_\mu = 190$ GeV in a 6 months data taking period,

Q^2 \ x_{bj}	0.05 $\pm$0.02	0.1 $\pm$0.03	0.2 $\pm$0.07
2 ± 0.5	40230 evts	35586 evts	39438 evts
3 ± 0.5	15438 evts	10158 evts	11550 evts
4 ± 0.5	8232 evts	4542 evts	4734 evts
5 ± 0.5	(5886) evts	2706 evts	2322 evts
6 ± 0.5	(3498) evts	1837 evts	1428 evts
7 ± 0.5	(2568) evts	1194 evts	966 evts

2. for μ^+ or μ^- at $E_\mu = 190$ GeV in a 3 months data taking period,

Q^2 \ x_{bj}	0.05 $\pm$0.02	0.1 $\pm$0.03	0.2 $\pm$0.07
2 ± 0.5	(35750) evts	26000 evts	33370 evts
3 ± 0.5	(15500) evts	8300 evts	9600 evts
4 ± 0.5	(11850) evts	(4000) evts	4000 evts
5 ± 0.5	(7800) evts	(2600) evts	2100 evts
6 ± 0.5	(4730) evts	(2310) evts	1300 evts
7 ± 0.5	(2120) evts	(2340) evts	920 evts

The distribution of the numbers of events reflects the decrease of the cross section when Q^2 and x_{Bj} increase. The numbers presented between two parentheses indicate a significant contamination of the BH process. At $E_\mu = 100$ GeV and $x_{Bj} \leq 0.1$ the BH-DVCS interference offers the opportunity to measure directly the DVCS amplitude.

It is clear that we have to demonstrate the relevance of our result within its statistics compared with different predictions and with the results obtained in other facilities. This work will be undertaken as soon as possible and is necessary to clarify the situation and reinforce the necessity of a DVCS experiment at COMPASS.

3.2 Experimental procedure

3.2.1 kinematics

In the range of the kinematics chosen for this DVCS study, the outgoing muon is emitted at a forward angle between 6 and 15 mrad, while the virtual photon varies from 2 deg to 15 deg. At small transfer, the photon has a large momentum and is focused inside a cone of small half-angle around the direction of the virtual photon, while the proton has a small momentum (limited in our experiment between 250 MeV/c and 750 MeV/c) and is rather focused on a cone of an half-angle larger than 50 deg around the direction of the virtual photon. The kinematics of proton and photon in the laboratory are reproduced in Fig. 7. This will fix the design of the photon and proton detectors.

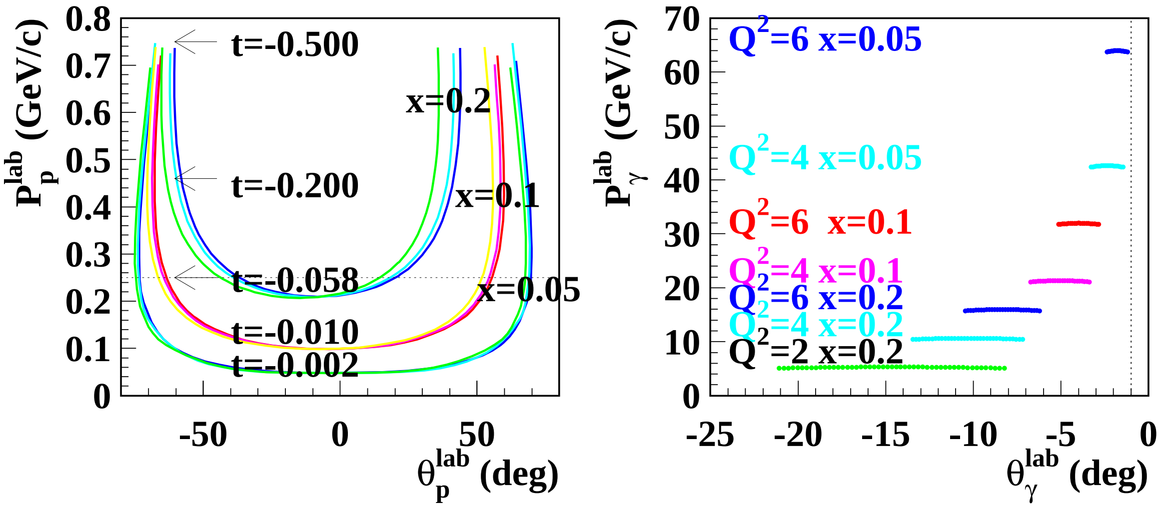

Figure 7: *Kinematics of the outgoing proton (focused in the backward direction) and of the outgoing photon (focused in the forward direction). The different curves at each x_{Bj} in the left figure are for $Q^2 = 2, 4, 6\ GeV^2$.*

3.2.2 The competing reactions

Two competing reactions constitute the main pollution of a clear selection of a DVCS event. They are represented in Fig. 8.

Deep π^0 production
π^0 production in the Deep regime brings into play the vector GPDs (H and E). Due to its small mass, the π^0 is kinematically very close to the DVCS photon. The π^0 decays in two photons: the higher energy photon has an energy between $E_{\pi^0}/2$ and E_{π^0} and is confined into a cone of half-angle m_{π^0}/E_{π^0} around the π^0 direction. As a result this photon resembles extremely a DVCS photon. The lower energy photon lies outside this cone; its energy varies from $E_{\pi^0}/2$ (on the cone) to 0 (in the backward direction comparatively to the incident π^0). Due to the Lorentz boost this low energy photon has a very high probability to be in the forward direction with a sufficiently high energy to be detected. The strategy in order to evaluate this contribution is then to detect the two photons of the π^0 decay in a forward detector. The π^0 decay is isotropic in its centre of mass, and so the corresponding "loss" due to the non-detection of one of the two photons of the π^0 decay can be perfectly estimated. This problem concerns the design of the forward photon detector and its adequate granularity.

The pion production in Associated DVCS
The final DVCS nucleon may turn into a resonance, i.e. the Δ resonance, which decay produces a pion. The physics contents of the Associated DVCS process is as important as the one of DVCS process. It gives access to some of the $N \to N^*$ transition GPDs [12]. Close to the pion threshold, a low energy theorem can be built to relate the $p \to N\pi$ GPDs to the elastic GPDs [31]. The soft π^0 can be emitted in all the directions.

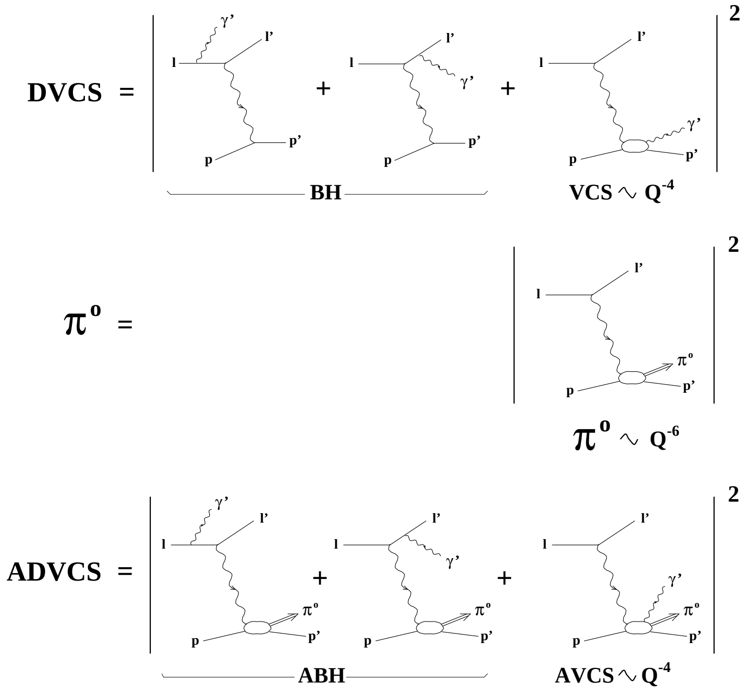

Figure 8: *Lowest order diagrams of competing reactions: DVCS, Deep π^0 production, Associated DVCS when the outgoing recoil proton is associated with a soft π^0.*

3.2.3 Missing mass exclusivity: not adapted

A tricky and economic way to select clearly a DVCS event is to detect the outgoing muon and photon which are of large energy and focused in the forward direction. A good separation in missing mass square between a DVCS event and an Associated DVCS event is of the order of $(m_p + m_{\pi^0})^2 - m_p^2 \simeq 0.25$ GeV^2. The resolution in missing mass depends on the resolutions of incident and outgoing muons and photons.

$$\Delta M_x^2 = \frac{\partial M_x^2}{\partial P_\mu} \cdot \frac{\Delta P_\mu}{P_\mu} \cdot P_\mu + \frac{\partial M_x^2}{\partial P_{\mu'}} \cdot \frac{\Delta P_{\mu'}}{P_{\mu'}} \cdot P_{\mu'} + \frac{\partial M_x^2}{\partial P_\gamma} \cdot \frac{\Delta P_\gamma}{P_\gamma} \cdot P_\gamma + ...$$

The dotted points represent the contribution of all the derivatives with the muon and photon angles which are negligible comparatively to the other terms in all the proposed experiments at small transfer. The two first terms show that the missing mass resolution is about proportional to the energy of the incident and outgoing leptons and so it is about 10 times larger at a facility of 200 GeV beam than at a facility of 20 GeV beam. The following resolutions of the COMPASS set-up for muons and photons (detected in a lead glass electromagnetic calorimeter) are $\Delta P_\mu/P_\mu = \Delta P_{\mu'}/P_{\mu'} = 4.10^{-3}$ and $\Delta P_\gamma/P_\gamma = 0.055/\sqrt{P_\gamma} + 0.015$. The contributions to the missing mass of the incident muon, outgoing muon, outgoing photon are 1.4, 1.4, 0.8 GeV^2 respectively at kinematics $Q^2 = 3$ GeV^2 and $x_{Bj} = 0.1$ and give a global resolution of 2 GeV^2. The missing mass technique is then useless with the high energy lepton beam.

3.2.4 Solution of a hermetic detector

Therefore a solution is to detect and identify the complete final state of the reaction and to design a detector to insure the exclusivity of the reaction. This can be achieved with the use of a hermetic detector and extensive veto systems.

The set-up we considered for these studies is represented in Fig. 9 and 13. The muons scatter off a 2.5 m long hydrogen target. The scattered muon is at an angle below 15 mrad and will be detected using the SAT. The outgoing photon lies at an angle below 350 mrad and will be detected in electromagnetic calorimeters. The great novelty, which is being studied and designed is the use of a recoil detector to identify and measure the momentum of the scattered proton. In addition, this recoil detector will be required to insure the exclusivity of the reaction and will therefore detect charged and neutral particles over the whole acceptance.

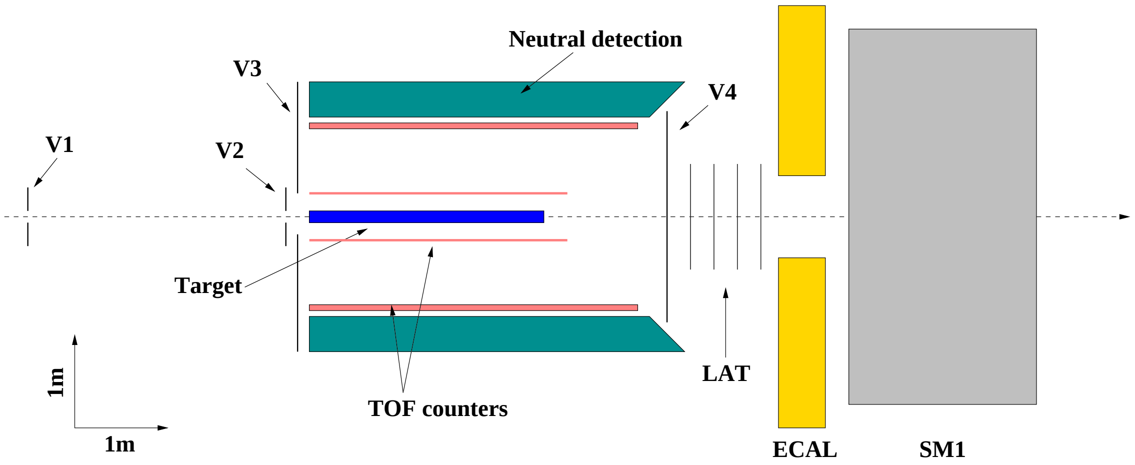

Figure 9: schematic drawing of the DVCS detector upstream from SM1.

For the purpose of defining the geometry and the operational conditions, we used the event generation program Pythia 6.1 [28]. This program includes most of the known processes [29] such as Deeply Inelastic Scattering and Deeply Meson Production. Among these processes, events with few particles in the final state might have a non negligible chance to be registered as DVCS. The experimental parameters such as maximum angle for photon detection, energy threshold for photon detection and maximum angle for charged particle detection could then be tuned (see Fig. 10). With photon detection extended up to 40 degrees and above an energy threshold of 50 MeV and with charged particle detection up to 30 degrees, we observe that hard processes have a probability of 4.5 10^{-5} to pass cuts. With these conditions, DVCS as estimated with models is more than an order of magnitude larger than hard processes over the whole useful Q^2 range (Fig. 11).

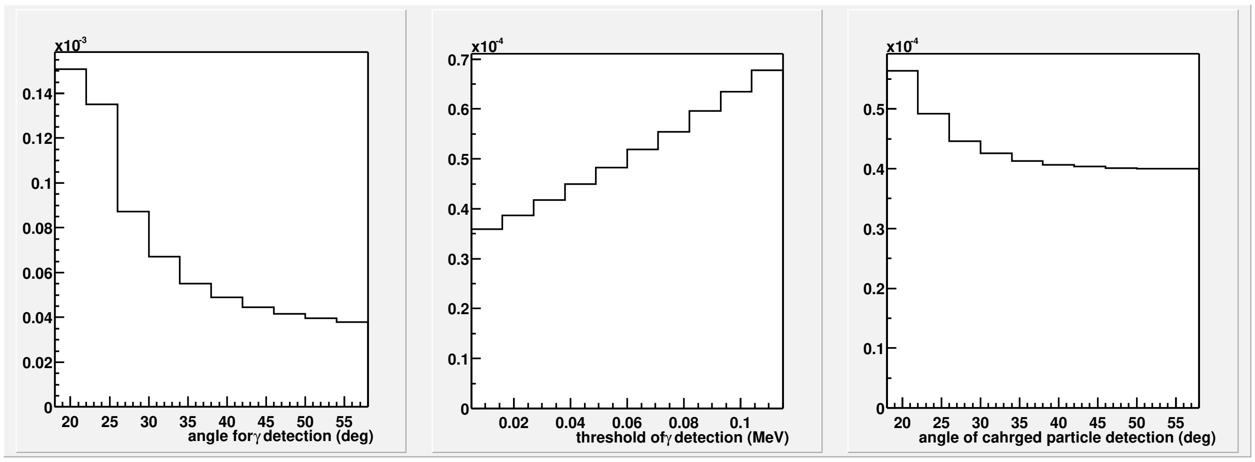

Figure 10: Probability for "hard processes" (generated with Pythia 6.0) events to pass cuts as a function of some experimental parameters : (a) angle for photon detection, (b) threshold for photon detection, (c) angle for charged particle detection. When varying one parameter the other two are kept at their nominal value (40 deg., 50 MeV, 30 deg. respectively).

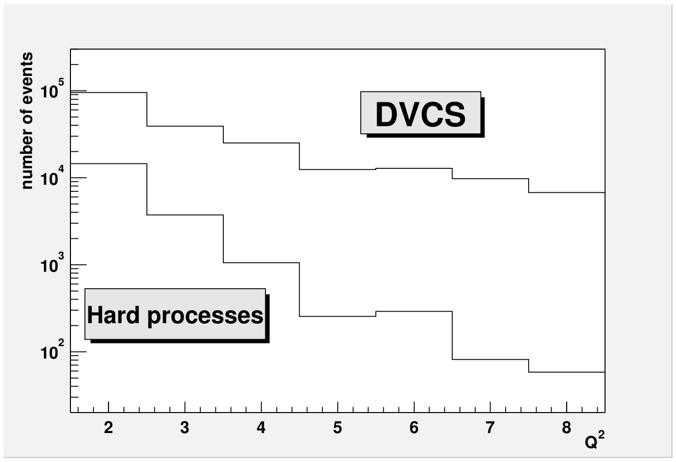

Figure 11: Number of events for DVCS and hard processes as a function of Q^2 for a 6 month running with 100 % efficiency.

3.3 Muon detection and resolution in Q^2 and x_{Bj}

In the chosen kinematical domain, $0.03 \leq x_{Bj} \leq 0.27$ and $1.5 \leq Q^2 \leq 6.5\mathrm{GeV}^2$ the outgoing muon is emitted between 6 and 15 mrad. It is mostly registered by the trigger hodoscope H' [30].

A complete simulation has been performed to determine the resolution in Q^2 and x_{Bj}. The geometry for the muon detection is indicated in Fig. 12. We consider a liquid Hydrogen target of 2.5 meter length, and the consequent energy losses and Coulomb multiple scattering. The incident muon beam has an energy ranging from 185 to 195 GeV defined with a resolution of 4.10^{-3}, a divergence of 1 mrad and a transverse size $\sigma(x) = \sigma(y) = 1.5$ cm. The outgoing muon is measured by a spectrometer dipole magnet SM2 placed in the forward direction at 15.5 m from the centre of the target and by 3 stations located downstream and 3 upstream at the position 9.1, 13., 15.2, 19.5, 19.8 and 31.8 m. Each station is supposed to have a resolution of 75 μm. The resulting resolutions on the outgoing muon are: $\sigma(P_{\mu'})/P_{\mu'} \simeq 4 \cdot 10^{-3}$, $\sigma(\theta_{\mu'}) \simeq 30$ μrad for a scattering angle of the order of 10 mrad.

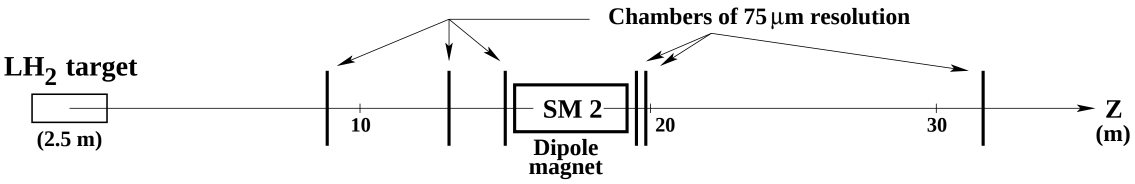

Figure 12: *Detection for the incident and going muons.*

For this device, the resolution $\sigma(Q^2)/Q^2 \simeq 1\%$ is found almost constant in the investigated range and the resolution $\sigma(x_{Bj})$ varies as indicated in the following table:

	x_{Bj}=0.05	x_{Bj}=0.1	x_{Bj}=0.2
Q^2=3	$\sigma(x_{Bj}) = 0.0011$	$\sigma(x_{Bj}) = 0.0048$	$\sigma(x_{Bj}) = 0.019$
Q^2=5	$\sigma(x_{Bj}) = 0.0006$	$\sigma(x_{Bj}) = 0.0028$	$\sigma(x_{Bj}) = 0.011$

The width of each bin in x_{Bj} is fixed to about 4 times the obtained resolution.

The transverse extension of the chamber placed at 30 meters is not sufficient to intercept outgoing muon at $x_{Bj} \leq .05$ or $Q^2 \geq 6GeV^2$. We will study the consequent effect on the resolution with standard wire chambers.

3.4 Reorganization of the forward photon detector

The goal of the electromagnetic calorimeter is to match as well as possible the kinematical phase space of the outgoing photon as it is presented in Fig. 7. We can consider two domains of detection:
domain I: 1 deg. $\leq \theta_\gamma \leq 8$ deg. and $P_\gamma \leq 64$ GeV/c
domain II: 8 deg. $\leq \theta_\gamma \leq 20$ deg. and $P_\gamma \leq 16$ GeV/c

The COMPASS set-up is already instrumented with two electromagnetic calorimeters ECAL1 and ECAL2 [32, 33]. They are mainly constituted of lead-glass blocks called GAMS. They are cells of $38.4 \times 38.4 \times 450$ mm^3. Typical characteristics of such calorimeter are:
- energy resolution: $\sigma P_\gamma / P_\gamma = 0.055/\sqrt{P_\gamma} + 0.015$
- position resolution: $\sigma_x = 6.0/\sqrt{P_\gamma} + 0.5$ in mm
- high rate capability: 90% of signal within 50ns gate with no dead time
- effective light yield: about 1 photoelectron per MeV; hence low energy photons of down 20 MeV can be reconstructed.

The separation of the overlapping electromagnetic showers in the cellular GAMS calorimeter is carefully studied in the Ref. [34]. The minimum distance between 2 photons of π^0 decay is $D = 2m_{\pi^0} Z/E_{\pi^0}$ where Z is the distance from the decay point to the calorimeter. The result of the study shows that at 10 GeV we reach a 50% level of the separation efficiency for D=1.9 cm (with a probability to find a false gamma smaller than 0.5%), and a 100% level for D = 4 cm. The last value is sightly shifted to D = 5 cm at 40 GeV.

The separation of two photons is a necessary requirement for the DVCS study and the good rejection of Deep π^0 production. ECAL1 is located at 13m from the centre of the hydrogen target (see Fig. 13) and can then be a very adequate calorimeter for the high energy photon up to 70 GeV (domain I). The size of ECAL1 allows to reach an acceptance of the order of 8 deg. However half of the total surface of ECAL1 is instrumented by larger size lead glass blocks ($143 \times 143 \times 450$ mm^3) from the OLGA calorimeter and would have to be changed for GAMS. Moreover the center hole is of the order of 2 deg., and it would be better to cover the angular range down to 1 deg.

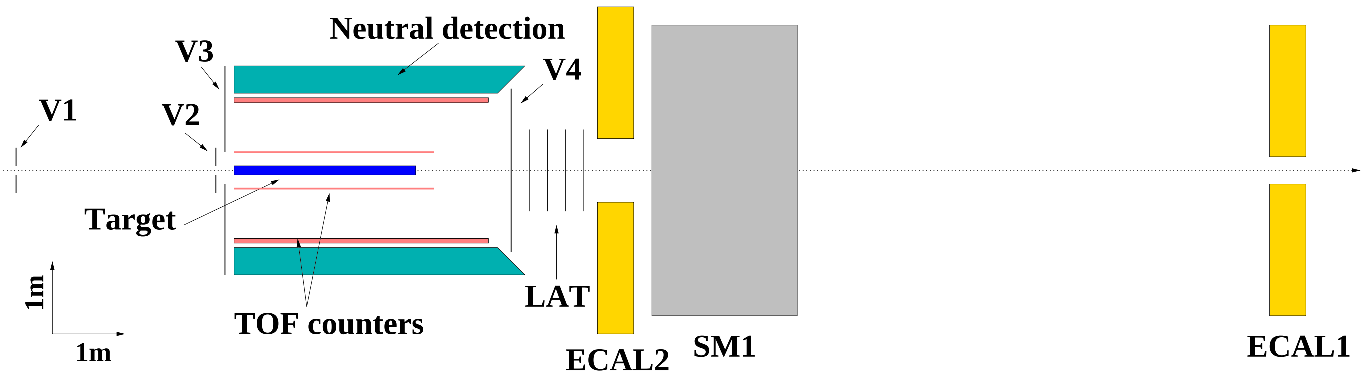

Figure 13: *Global set-up with the position of the electromagnetic calorimeter, ECAL2 at 3m and ECAL1 at 13m upstream from the target in order to provide a good detection of photons in a large forward acceptance.(Note that all the standard COMPASS equipments are present and located at their normal position. Only the space upstream from SM1 is differently instrumented.)*

To obtain a good angular coverage of the outgoing photons of moderate energy (domain II), it is sufficient to use ECAL2 positioned at 3m from the end of the target just upstream from SM1 (see Fig. 13). The minimum vertical angle is 18 deg. while the minimal horizontal angle is 23 deg. With the extension provided by the additional lead-glass blocks ($75 \times 75 \times 360$ mm^3) from the WA89 experiment, we have a coverage of 36 deg. horizontally which is completely useful to detect at maximum a second photon and decrease the background as it was mentioned in the subsection 3.2.4.

This scenario with the two electromagnetic calorimeters, placed at 3m and 13 m from the target, provides a solution for the detection of DVCS photons in a reasonably large forward acceptance.

3.5 Recoil detector and hodoscope for hermeticity

3.5.1 Objectives

The requirements of the recoil detector presented earlier can be summarized as follows:

- detection of the recoil proton between 30 and 80 degrees and measurement of its momentum in the range 250 to 750 MeV/c with a resolution of 2% to get a 4% resolution on t.
- discrimination between proton and $\pi^{\pm}$.
- ability to detect photons and neutrons with some efficiency.
- guaranty of the exclusivity of the DVCS reaction.

This part of the detector will be the core of the detection apparatus and will demand a major development. Studies based on an existing recoil proton detector [36] are in progress. At present time, we consider a detector constituted of several segmented cylindrical layers of scintillator counters with two end photomultiplier (PMT) read-out. Fig. 14 represents a half longitudinal section of the different layers.

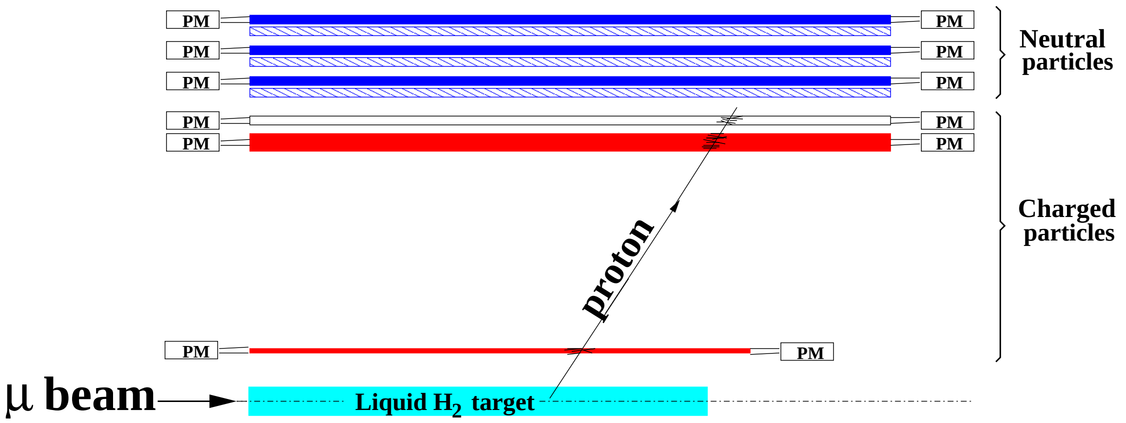

Figure 14: Half longitudinal section of the different layers that a particle will encounter after leaving the hydrogen target.

3.5.2 Detection of protons and pions at large angle

The momentum of the particle is determined from the time of flight measurement between the first two cylindrical layers of scintillating counters separated by 90 cm. The length of the inner barrel must be of the size of the hydrogen target (2.5 m) while the length of the outer barrel must be of the order of 3.5 m in order to get the expected angular coverage. The thickness of the first layer of scintillators has to be as thin as possible (typically 4 mm) in order to allow low momentum particles to pass through. The thickness of the second layer of scintillators (5 to 10 cm) has to be a compromise between the stopping power of low momentum particles and the best collection of scintillation light for a better timing resolution. The PMT signals collected at both ends of the scintillator counters will give the particle position and angle. Typical resolution of 350 ps on the time of flight can be obtained. When associated with an outgoing muon detection it will provide a longitudinal vertex resolution of 2 cm ($\sigma_\perp = 0.25$ cm). Each scintillator will cover an azimuthal angle range of $\pi/3$ for the inner barrel and about $\pi/16$ for the outer one. This segmentation will not only decrease the rates for the counters close to the beam but it will also allow to refine the tracking of the proton and to determine the ϕ angular distribution.

A first level GEANT simulation shows that momentum resolution of a few % can be achieved in our kinematical range with a proton reconstruction efficiency around 80% using the correlation between the energy loss in the layers of scintillator and the velocity β of the particle through minimization algorithms.

3.5.3 Detection of neutral particles at large angle

A possible detector for neutral particles such as photons (from π^0 decay) and neutrons (from Δ decay) could be made of a sandwich of lead and scintillator alternating layers. A comparable detector (3 layers, 5 mm of Pb and 5 mm of scintillator) was built [36] and detection efficiencies of 50% for photons and of 15% for neutrons were obtained. This can certainly be improved by taking thiner slices and increasing the number of sampling layers.

3.5.4 Veto system

We will use the existing veto system to reject the "near halo" (V1 and V2 on Fig. 9). We will add a "far halo" veto (V3) composed of scintillating counters upstream of the recoil detector and covering the whole cross-section of the detector. For the identification of the DVCS process, one will need to reject events with charged particles in the forward direction. This can be done using an array of scintillating counters (V4) located after the recoil detector. This detector needs to be added because the coverage of the existing chamber is not adapted and because the occupancy rate in the drift chambers is of the order of 3 tracks per event [37]. Detection of charge particle at larger angle and rejection of non-proton events will be performed using the recoil detector as shown previously.

Unfortunately, the forward veto could also reject DVCS events be they accompanied by electromagnetic background. For each DVCS event the incoming and scattered muons will interact in the target through elastic scattering off the electrons of the hydrogen atoms. Using GEANT, we found that 10 % of the DVCS events will have at least one hit in the veto and will be rejected. At larger angle, the same studies have shown that an average multiplicity of 1.6 is to be expected in the inner TOF counters. These spurious hits can still be rejected thanks to the segmentation and to the vertex resolution.

3.6 Experimental tests of proton detection

We have tested the feasibility of the proposed detection of the recoil protons. This was performed in the COMPASS environment under real beam conditions (halo, secondary particle productions, hadron contaminations...) at the nominal beam intensity of $2.\,10^8$ muons per spill (2.2 seconds long). This was done in summer 2000 with a simplified Time Of Flight set-up (Fig. 15) which was a scale 1 sector of detection system described

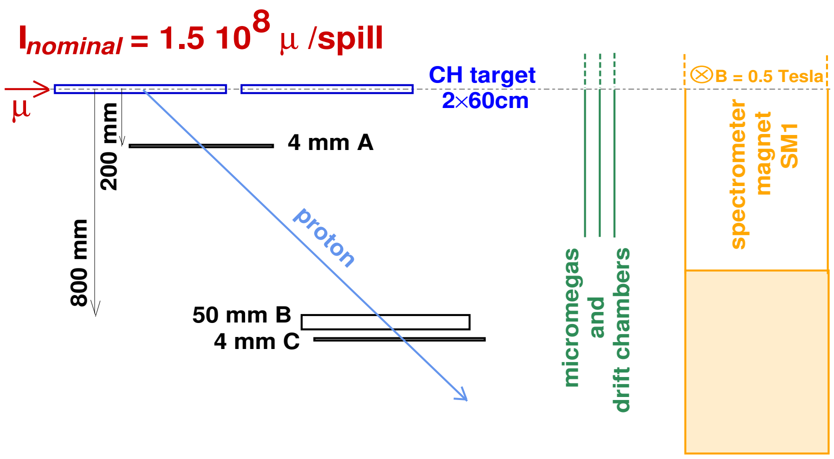

Figure 15: Test set-up for proton detection.

above. We used three scintillator layers (read at both sides) : a 4 mm thick one close to the target (A), a 5 cm thick one at 80 cm from the target (B) and another thick scintillator right after B (C). A 60 cm long polyethylene target was used, which is equivalent to 3.5 times more material than the foreseen liquid hydrogen target.

The rate observed in the scintillator close to the target is of the order of 2 MHz above a minimal threshold (1/10 of MIP deposited energy). As it is an overestimate, it demonstrated that the background environment was acceptable for the TOF system. This rate is also of the same order of magnitude than the one expected for electromagnetic background coming mostly from μe scattering.

The results obtained with this setup (see Fig. 16) show a clear proton signal even though most of the hits are coming from pions and electrons. The usual shape of the plot ΔE versus β allows to distinguish protons that are stopped or not in B. The momentum range in which protons are identified is from 320 to 620 MeV/c ($\beta =$ 0.2 and 0.55 respectively) and is close to the goal of the DVCS experiment. With a refined trigger that rejected most of the pions and electrons and looking only at events

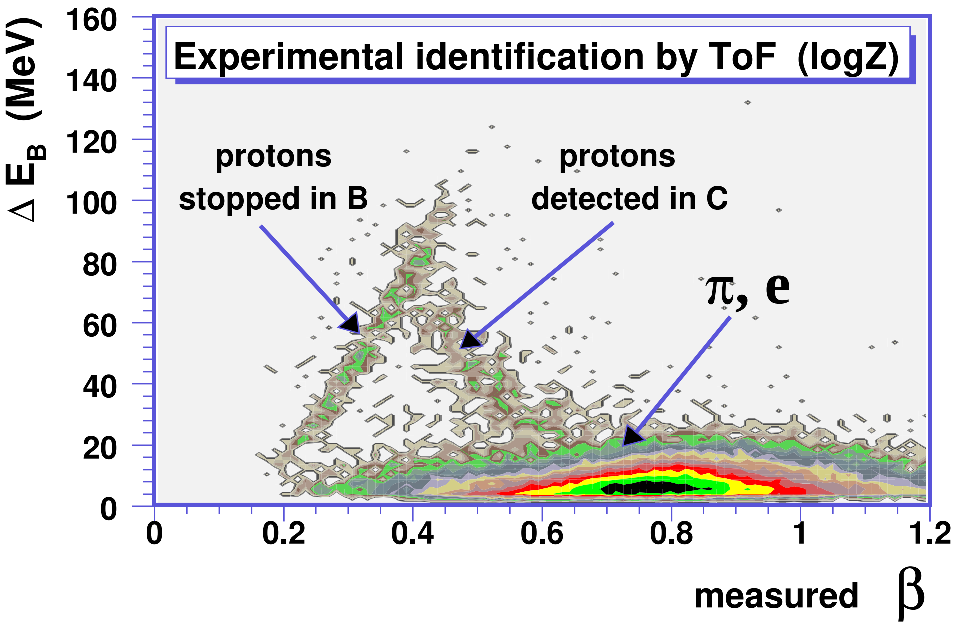

Figure 16: Energy loss in the thick scintillator as a function of the β measured using Time of Flight. The color scale is logarithmic.

that were stopped in B (all kinetic energy is deposited) it was possible to determine the mass distribution of the scattered particle (see Fig. 17) which shows that a clear proton signal can be observed as well as a faint deuteron signal.

These tests have demonstrated that the detection of protons under the real COMPASS conditions is feasible. Further tests are foreseen in order to improve on the detection efficiency and on the particle identification over a wide range in β and also to detect a proton in coincidence with the existing COMPASS μ trigger.

3.7 Conclusion

This draft is an attempt to define the outline of a DVCS experiment at COMPASS which takes advantage of the high energy of the muon beam and the large domain in Q^2 and x_{Bj}. This study will certainly be improved by the expertise of the collaboration. Complementary studies on deep meson production have to proceed in order to determine the optimized COMPASS set-up and to enlarge the scope of the experiment with respect to the physics of the GPDs.

In the next coming year, a large effort has also to be pursued to demonstrate the impact of the result within statistics in order to reinforce the motivations of the COMPASS experiment.

Some encouraging results have been obtained for recoil proton detection in the COMPASS environment. They have to be pursued. The next steps will focus on the study the proton detection efficiency, the coincidence of a recoil proton with a muon, and finally also with a photon.

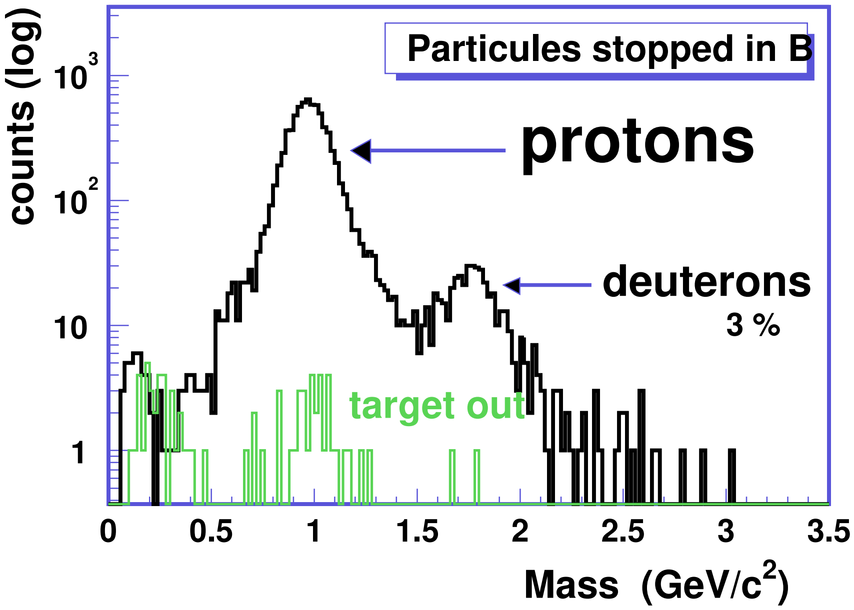

Figure 17: Mass distribution of particles stopped in the B scintillator for the CH target in and out.

References

[1] X. Ji, Phys. Rev. Lett. **78**, 610 (1997); Phys. Rev. D **55**, 7114 (1997).

[2] A.V. Radyushkin, Phys. Rev. Lett. B **380**, 417 (1996); Phys. Rev. D **56**, 5524 (1997).

[3] J.C. Collins, L. Frankfurt and M. Strikman, Phys. Rev. **D56**, 2982 (1997).

[4] M. Diehl, hep-ph/0010200.

[5] M. Burkardt, hep/0105234.

[6] B. Pire and J. Ralston, private communication.

[7] X. Ji, W. Melnitchouk and X. Song, Phys. Rev. **D56**, 5511 (1997).

[8] V.Y. Petrov, P.V. Pobylitsa, M.V. Polakov, I. Börnig, K. Goeke, C. Weiss, Phys. Rev. **D57**, 4325 (1998).

[9] M. Diehl, T. Feldmann, R. Jakob and P. Kroll, Eur. Phys. J. **C8**, 409 (1999).

[10] M. Vanderhaeghen, P.A.M. Guichon, Prog. Part. Nucl. Phys., Vol. 41, 125 (1998); M. Vanderhaeghen, P.A.M. Guichon, M. Guidal, Phys.Rev. **D 60**, 094017 (1999).

[11] A.V. Radyushkin, Phys. Lett. **B449**, 81 (1999); hep-ph/0101225.

[12] K. Goeke, M. Polyakov and M. Vanderhaeghen, hep-ph/0106012.

[13] X. Ji, J. Phys. **G 24**, 1181 (1998).

[14] L. Mossé, P.A.M. Guichon and M. Vanderhaeghen, private communication.

[15] J. Pochodzalla, L. Mankiewicz, M. Moinester, G. Piller, A. Sandacz and M. Vanderhaeghen, submitted to 6th INT / Jlab Workshop on Exclusive and Semiexclusive Processes at High Momentum Transfer, Newport News, VA, 19-23 May 1999, hep-ex/9909534.

[16] A. Sandacz, presented at the Physics Workshop during the COMPASS week, Munich 1999, COMPASS Note 2000-1.

[17] P.R.B. Saull for the ZEUS Coll., Prompt photon production and observation of Deeply Virtual Compton Scattering, EPS-HEP99, Tampere 1999, hep-ex/0003030.

[18] L. Favart for H1 and ZEUS Coll., Deeply Virtual Compton Scattering at HERA, ICHEP 2000, Osaka, hep-ex/0101046;
C. Adloff *et al.*, H1 Collaboration, Measurement of Deeply Virtual Compton Scattering at HERA, hep-ex/0107005, submitted to Physics Letters B

[19] A. Airapetian *et al.* (HERMES Collaboration), Eur. Phys. J. **C17**, 389 (2000).

[20] M. Amaryan for HERMES Coll., deeply Virtual Compton scattering and exclusive meson production at HERMES, talk at the workshop on Skewed parton distributions and lepton-nucleon scattering, http://hermes.desy.de/workshop/TALKS/talks.html.

[21] M. Guidal, M. Garcon, E. Smith *et al.*, CEBAF proposal 99-105 (1999).

[22] P.Y. Bertin, C. Hyde-Wright, F. Sabatie *et al.*, CEBAF proposal 00-110 (2000).

[23] L. Elouadrhiri, S, Stepanyan, V. Burkert, M. Garçon *et al.*, CEBAF proposal 01-113 (2001).

[24] S. Stepanian *et al.*, in preparation for Phys. Rev. Lett.

[25] M. Diehl, T. Gousset, B. Pire, J.P. Ralston, Phys. Lett. **B411**, 193 (1997).

[26] http://proj-cngs.web.cern.ch/proj-cngs/cngs.htm.

[27] Lau Gatignon, private communication.

[28] Pythia 6.1 User's manual, hep-ph/0010017.

[29] C. Friberg and T. Sjöstrand, hep-ph/0007314.

[30] J. Pretz, Geometrical Trigger acceptance in the COMPASS set-up, December 6,2000.

[31] L. Mossé, P.A.M. Guichon and M. Vanderhaeghen, private communication.

[32] A Proposal for a Common Muon and Proton Apparatus for Structure and Spectroscopy, CERN/SPSLC 96-14.

[33] V. Poliakov, Presentation of ECAL1 and ECAL 2, January 25, 2001.

[34] A. A. Lednev, Separation of the overlapping electromagnetic showers in the cellular GAMS-type calorimeters, Preprint IHEP 93-153 (1993), Protvino, Russia.

[35] S. Keller et al., Nucl. Instr. Meth. A **419**, 382 (1998); B. Schmidt, Nucl. Instr. Meth. A **419**, 230 (1998).

[36] D. Alde et al, Nucl. Instr. Meth. A **342**, 389 (1994).

[37] J.M. Legoff, private communication.

[38] G. Audit et al, Nucl. Instr. Meth. A **301**, 473 (1991).

[39] A. Braghieri et al, Nucl. Instr. Meth. A **343**, 623 (1994).